Measuring Speed of Light Using Electron-Positron Annihilation Through Decay of ^{22}Na

Isaiah Mumaw* and Jordan Burhanna†
University of Notre Dame
Advanced Physics Lab
(Dated: April 12, 2022)

We placed a small sample of ^{22}Na, a material subject to β^+ decay due to its excess of protons, between two opposing scintillators connected to photomultiplier tubes. The positrons produced in β^+ decay interact with the environment surrounding the sample, colliding with electrons and annihilating. This releases a pair of photons moving in opposing directions with equal energies. As these hit the detectors, we calculated the time differential between each collision and used this time difference, along with the sample position relative to the detectors, in order to calculate the speed of light. Our resulting calculation gave a value of $c_{\text{exp}} = (2.9279 \pm 0.0863) \times 10^8 \ \frac{\text{m}}{\text{s}}$, roughly 2.3% below the established speed of light, differing by 1σ. This was an improvement from the work done in the previous semester, which had a value roughly 5.3% above the established value, and differing by 4σ.

I. BACKGROUND

A. Speed of Light

The speed of light in a vacuum, represented by c, is a physical constant representing the speed of electromagnetic radiation in a vacuum. Mathematically, it is defined as:

$$c = \frac{1}{\sqrt{\epsilon_0 \mu_0}}, \tag{1}$$

where ϵ_0 represents the vacuum permittivity and μ_0 represents the magnetic permeability. This comes out to exactly 299792458 meters per second [1].

According to Einstein's theory of special relativity, this velocity is universal in all inertial reference frames, and represents an upper bound to the velocity of all physical objects. All photons travelling in a vacuum will have exactly this velocity [1].

B. Beta Plus Decay

Beta (β) decay is a form of radioactive decay whereby an unstable nucleus releases a beta particle and corresponding neutrino, converting it into a more stable isobar. It has two forms: β^- and β^+ [2].

In β^+ decay, a proton (comprised of two up quarks and a down quark) is converted to a neutron (comprised of one up quark and two down quarks). This occurs through the weak interaction, flipping one of the up quarks in the proton to a down quark and releasing a W^+ boson in order to account for the energy difference. This boson rapidly decays into an e^+ and a ν_e, with the general form of this process being given as:

$${}^{A}_{Z}X \rightarrow {}^{A}_{Z-1}X' + e^+ + v_e. \tag{2}$$

Generally speaking, β^+ decay occurs in proton-rich nuclei, with the resulting nucleus having a greater binding energy [2]. The Feynman diagram for this process can be viewed in Fig. 1.

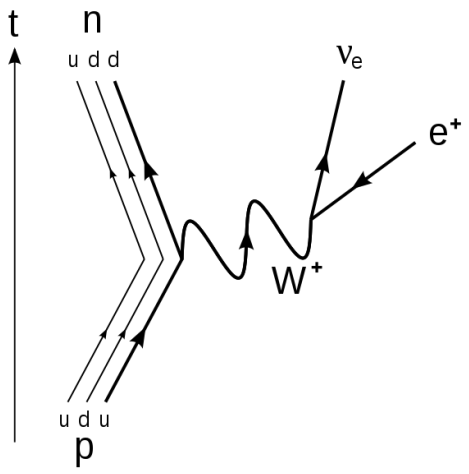

FIG. 1. Feynman Diagram for β^+ Decay. Due to weak interaction, a proton flips to a neutron, with the energy difference being accounted for by emission of an e^+ and ν_e [3].

C. Electron-Positron Annihilation

Electron-positron annihilation occurs when an electron (e^-) encounters its antiparticle, a positron (e^+). This interaction produces two photons. Due to the conservation laws of energy and momentum, these photons have equal

* imumaw@nd.edu
† jburhann@nd.edu

and opposite velocities, and energies of roughly 511 keV, which is equivalent to the $e^{\pm}$ rest mass [4]. The Feynman diagram for this process is shown in Fig. 2.

Mathematically, this process is given as [4]:

$$e^- + e^+ = \gamma + \gamma. \tag{3}$$

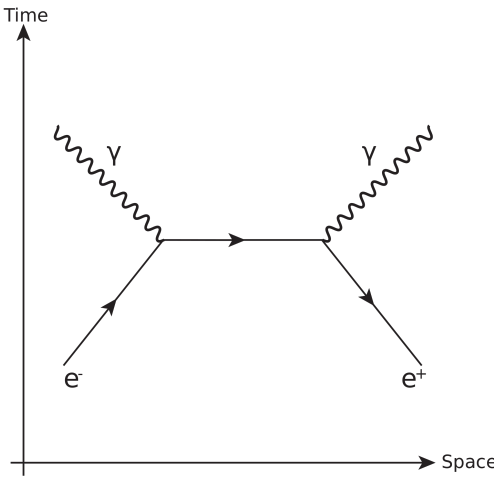

FIG. 2. Feynman Diagram for electron-positron annihilation. The two emitted photons have energies of 511 keV and have equal and opposite momenta [5].

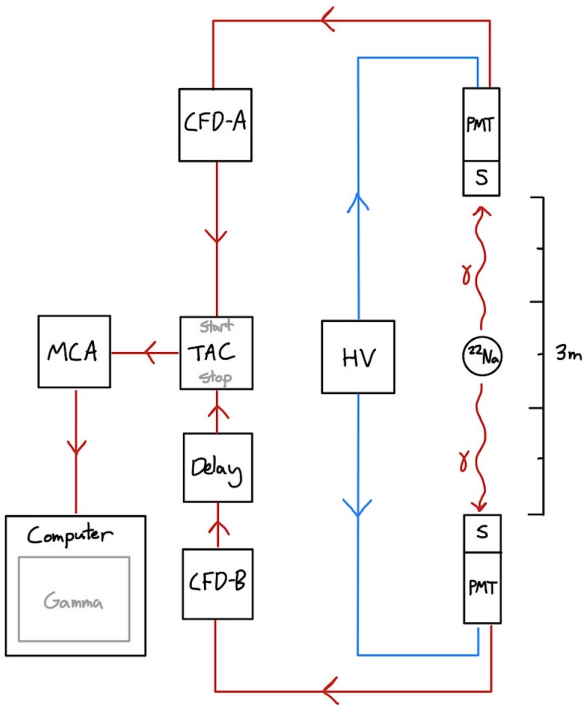

FIG. 3. Block diagram of experimental setup. Signals from incoming photons are separated from environmental noise and separated into channels based on the time difference between the pairs.

II. EXPERIMENTAL SETUP

The source for this experiment was a sample of ^{22}Na, placed along a 3 meter track. ^{22}Na is an unstable, man-made isotope, with a half-life of 2.6 years. It decays according to Eq. 2 into ^{22}Ne, emitting e^+ that undergo annihilation as they interact with the surrounding environment, producing a photon pair.

At each end of the track is a scintillator (S) connected to photomultiplier tube (PMT). Produced photons have a small probability of hitting one or both of these detectors, varying depending on the position of the sample along the track. Both detectors are powered with a high voltage source (HV).

Each detector's output is connected to a Constant Fraction Discriminator (CFD-A and CFD-B) in order to isolate the desired photon energy of 511 keV, as is produced in these types of annihilations. CFD-A's output is sent directly to the start input for the Time-to-Amplitude Convertor (TAC). CFD-B's output is additionally routed through a delay module to prevent signal overlap before being sent to the stop input of the TAC.

The time difference between the start and stop inputs of the TAC is converted to a voltage, varying based on the length of time between each signal. However, if a stop signal is not detected within 0.1 μs after the start signal, no voltage is sent.

TAC output is then routed through a multi-channel analyzer (MCA) in order to convert voltages into discrete signals that can be read by the computer. This resulting data was collected using Gamma Data Acquisition and Analysis.

III. RESULTS AND ANALYSIS

A. Photon Annihilation Data

Incoming data took the form of a narrow Gaussian, though there was an exponential-like modification to the data in the region where the time difference was less than the mean. Each trial lasted roughly 48 hours, with the sample moving 50cm between each trial. 5 trials were successfully completed.

To improve fitting, two filters were applied to the collected data prior to fitting. The first filter functioned as a band pass, isolating the true Gaussian portion of the data and setting the remaining channels to 0. The second filter functioned as a noise gate, setting channels below the threshold of 10 counts to 0.

Fit lines were calculated using a standard Gaussian distribution:

$$f(x, \mu, \sigma) = \frac{1}{\sigma\sqrt{2\pi}} e^{-\frac{1}{2}\left(\frac{x-\mu}{\sigma}\right)^2}, \tag{4}$$

where μ is the mean and σ is the standard deviation. Fitting parameters were determined in Python using the Scipy module. The fit method of this module minimizes the negative log-likelihood (NLL) function, decreasing its value as the data approaches the fit.

Fig. 4 shows the results from Trial 3, where the sample was equidistant from both detectors.

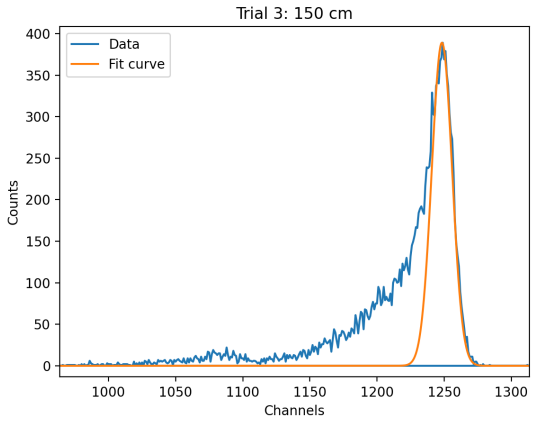

FIG. 4. Data from Trial 3. Extraneous noise has been filtered out using both band pass and noise gate methods, and the remaining data has been fit with a Gaussian distribution.

Table I shows the final calculated results from each trial after performing the fitting operations, as well as the distance of the sample from the left side of the track for each trial. These results are plotted in Fig. 5.

TABLE I. Results from each trial after filtering and fitting to Gaussian distribution.

Trial	Position (cm)	Mean (ch.)	Stnd. Dev. (ch.)
1	50	965.1596	8.5022
2	100	1106.9554	7.0378
3	150	1248.3720	7.5777
4	200	1388.4860	7.6227
5	250	1523.8026	7.5445

Linear regression was performed on these data points using Scipy's linregress. This gave a fit with $R^2 \approx 0.998$. The calculated slope represents m_d, the ratio between channels and distance, giving us:

$$m_d = 2.7976 \pm 0.0148 \ \frac{\text{ch}}{\text{cm}}, \tag{5}$$

where the uncertainty is calculated using the standard uncertainty of the slope for linear regression [6]:

$$\sigma_b = \sqrt{\frac{\sum (y_i - \hat{y}_i)^2}{(n-2)\sum (x_i - \bar{x})^2}}. \tag{6}$$

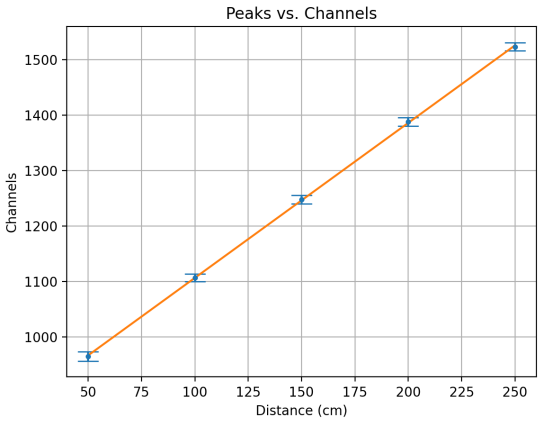

FIG. 5. Calculated mean channel for each trial, plotted against distance. Means and standard deviations were found by fitting to a Gaussian distribution.

B. Time Calibration Data

To convert m_d into the proper units for speed, a time calibration was performed. The module for this operation produced a series of narrow peaks with a period of 0.01 μs, as shown in Fig. 6.

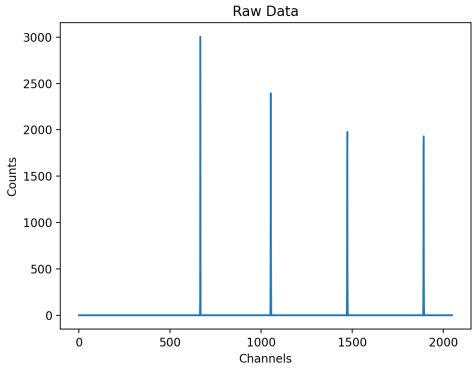

FIG. 6. Raw time calibration data using a period of 0.01 μs.

Each peak did have some variance to it, so the weighted average around each was calculated in order to find the precise peak position, with the error being given by the standard error of the weighted average.

Linear regression was performed over the time calibration data, giving a fit with $R^2 \approx 0.996$. The calculated slope represents m_s, the ratio between channels and time, giving us:

$$m_s = (4.0956 \pm 0.0564) \times 10^4 \ \frac{\text{ch}}{\mu\text{s}}, \tag{7}$$

where the uncertainty is again calculated using Eq. 6. All results for time calibration are shown in Fig. 7.

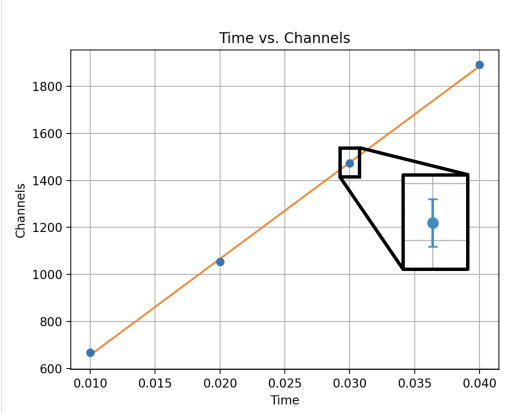

FIG. 7. Time calibration peaks vs time, where each peak channel was found using a weighted average. Error bars on this section were small due to the small variance of incoming data, and as such a zoomed-in image has been included.

C. Final Results

With m_d and m_s known, c_{exp} can be calculated through simple unit conversion (with an additional factor of 2 to account for travel time in both directions, and a factor of 1000 to convert to SI base units):

$$c_{\text{exp}} = 2 \times 1000 \times \frac{m_s}{m_d}. \tag{8}$$

This gives a final result of:

$$c_{\text{exp}} = (2.9279 \pm 0.0863) \times 10^8 \ \frac{\text{m}}{\text{s}}, \tag{9}$$

with the uncertainty being calculated according to standard error propagation of division/multiplication:

$$\sigma_{c_{\text{exp}}} = 2 \times c_{\text{exp}} \sqrt{\left(\frac{\sigma_{m_d}}{m_d}\right)^2 + \left(\frac{\sigma_{m_s}}{m_s}\right)^2}. \tag{10}$$

This result is within 1σ of the theoretical value of c.

D. Comparison to Previous Measurement

This experiment was previously conducted in the fall semester. Five trials were completed, though with markedly less spread on the distances between each trial.

In addition, the data analysis portion attempted to account for the non-Gaussian portion of the data by using an exponentially modified Gaussian function, given as:

$$f(x, K, \mu, \sigma) = \frac{1}{2K\sigma} \exp\left(\frac{1}{2K^2} - \frac{x-\mu}{K\sigma}\right) \times \text{erfc}\left(-\frac{\frac{x-\mu}{\sigma} - \frac{1}{K}}{\sqrt{2}}\right), \tag{11}$$

where μ is the centroid, σ is the variance, and K is the scaling factor. While this function did manage to account for some of the unexpected behavior, the calculated peaks at the location of interest were often very inaccurate and tended to unpredictably overestimate the true peak position. As such, this method introduced additional uncertainty and significant deviation that was not present in this iteration of the experiment.

The final calculation in the previous iteration gave:

$$c_{\text{exp}} = (3.15 \pm 0.04) \times 10^8 \ \frac{\text{m}}{\text{s}}. \tag{12}$$

This differed from c by roughly 4σ, overestimating by roughly 5.3%. The updated method in this version gave a result much closer to the theoretical value of c, instead *underestimating* by only 2.3%.

IV. DISCUSSION

The final calculated value for c_{exp} was within expectations for this experiment, having an expected range within 5.0% of c. The result was an improvement from the previous semester, decreasing the deviation by 3.0%, and decreasing the sigma value from 4σ to 1σ.

Error in this lab did unexpectedly arise due to the presence of non-Gaussian behavior with times less than the mean time. Expected results for this lab take the form of a Gaussian distribution, as ongoing electron-positron annihilation should produce a roughly equal distribution of photons in space. While it is possible to account for this discrepancy in the analysis process by ignoring channels displaying unexpected behavior, it is very likely that some information was lost as a result of this. It is unknown what could have caused this effect, and additional experimentation and testing will be necessary in order to mitigate its effects in the future.

While c has had a precise definition since the 1983, and has been made increasingly rigorous as of 2019 [7], increasingly advanced measurement techniques are still necessary in order to verify this value with the higher precision needed for cutting-edge scientific research. Experiments such as this continue to verify the validity of previous calculations, and also provide insight into other physical processes including annihilation and radioactive decay.

V. ACKNOWLEDGEMENTS

We extend our gratitude to the University of Notre Dame and its physics department for the use of their facilities while working on this experiment. We also thank Professor Zech and our TA Will von Seeger, for providing us with guidance and assistance throughout the process.

[1] Griffiths, D. J. (2017). *Introduction to Electrodynamics* (4th ed.). Cambridge University Press.

[2] Urone, P. P., & Hinrichs, R. (2012). *Nuclear Decay and Conservation Laws*. In College Physics. OpenStax.

[3] Linsell, R. (2014, March 30). *Beta Plus and Beta Minus Decay*. The Fizzics Organization. Retrieved Apr 1, 2022, from https://www.fizzics.org/beta-plus-and-beta-minus-notes-and-video-lesson/.

[4] Elbanan, M. (2012, January 19). *Electron-positron annihilation*. Radiopaedia. Retrieved Apr 1, 2022, from https://radiopaedia.org/articles/electron-positron-annihilation-1?lang=us.

[5] Manticorp. (2011, December 6). *Annihilation*. Wikipedia. Retrieved Apr 1, 2022, from https://en.wikipedia.org/wiki/Annihilation#/media/File:Mutual_Annihilation_of_a_Positron_Electron_pair.svg.

[6] Stone, D. C., & Ellis, J. (2013, October 25). *Statistics in Analytical Chemistry - Regression*. University of Toronto: Department of Chemistry. Retrieved Apr 3, 2022, from https://sites.chem.utoronto.ca/chemistry/coursenotes/analsci/stats/ErrRegr.html.

[7] NIST (2018, May 12). *A Turning Point for Humanity: Redefining the World's Measurement System*. National Institute of Standards and Technology. Retrieved Apr 4, 2022, from https://www.nist.gov/si-redefinition/turning-point-humanity-redefining-worlds-measurement-system